2013-10-24

Surface Photovoltage Characterization Of Organic Photovoltaic Devices

UTD AUTHOR(S): Yun-Ju Lee, Jian Wang and Julia W.P. Hsu

Surface photovoltage characterization of organic photovoltaic devices

Yun-Ju Lee, Jian Wang, and Julia W. P. Hsu

Citation: Applied Physics Letters **103**, 173302 (2013); doi: 10.1063/1.4827104
View online: http://dx.doi.org/10.1063/1.4827104
View Table of Contents: http://scitation.aip.org/content/aip/journal/apl/103/17?ver=pdfcov
Published by the AIP Publishing

Surface photovoltage characterization of organic photovoltaic devices

Yun-Ju Lee,[a] Jian Wang, and Julia W. P. Hsu
Department of Materials Science and Engineering, University of Texas at Dallas, Richardson, Texas 75080, USA

(Received 12 August 2013; accepted 13 October 2013; published online 24 October 2013)

Surface photovoltage response in bulk heterojunction organic solar cells is determined using a Kelvin probe with variable illumination intensity and wavelength. The effect of device architecture, carrier transport layers, donor:acceptor combinations, and device processing conditions are studied. We observe a positive (negative) surface photovoltage response, corresponding to efficient accumulation of electrons (holes) at the top electrode in conventional (inverted) devices. The linear relationship between surface photovoltage and log(intensity) and the agreement with open circuit voltage indicate that surface photovoltage magnitude quantifies the separation of photogenerated carriers in organic solar cells at open circuit condition. © *2013 AIP Publishing LLC*. [http://dx.doi.org/10.1063/1.4827104]

Organic solar cells (OSCs) represent a promising method toward low cost, lightweight renewable energy.[1,2] An important parameter in OSC performance is the open circuit voltage (V_{oc}), which is governed by the energy difference the ionization potential of the donor and the electron affinity of the acceptor.[3–5] Several additional factors also influence V_{oc} of OSCs, particularly those that use the bulk heterojunction (BHJ) active layer morphology. They include work function Φ of electrodes when in direct contact with the BHJ[6] and inclusion of interfacial contact layers between electrode and BHJ.[7–13] Surface photovoltage (SPV) measurement is a non-contact technique that has been used to characterize photoresponse of inorganic semiconductors.[14] When Kelvin probe technique is used, SPV measures the photoinduced shift in Φ of the top layer due to contributions from band bending at the surface and buried interfaces. Measured at the same illumination intensity, SPV and V_{oc} were found to correlate with each other for crystalline[15] and amorphous Si,[16] bilayer small-molecule,[17] and photoelectrochemical[18] solar cells, indicating that SPV measurement probes the quasi-Fermi level splitting under illumination at open circuit condition. Kronik *et al*. used SPV measurement to study the effect of Na concentration on CIGS solar cell performance.[19] More recently, atomic force microscope based scanning Kelvin force microscopy has been performed on active layers of BHJ organic and hybrid solar cells to study donor-acceptor phase separation.[20–23] Most of these reports focus on the high-resolution imaging of photoinduced charge separation within the active layer. In this Letter, we utilized the Kelvin probe technique with controlled illumination to measure the SPV response of BHJ OSCs with different carrier transport layers, donor:acceptor combinations, and thermal annealing conditions, and found a linear dependence between SPV and log(intensity), with the magnitude affected by the inclusion of carrier transport layers and the energy level offset between donor and acceptor. We also demonstrated agreement between SPV and V_{oc}, confirming that the Kelvin probe is a valuable tool to quantify the separation of photogenerated carriers in OSCs.

Inverted and conventional OSCs were fabricated using published recipes. For inverted devices,[9,24] the layer sequence consists of patterned ITO on glass (20 Ω/sq, thin film devices), 40 nm sol-gel ZnO electron transport layer (ETL), and 200 nm of 1:1 weight ratio poly(3-hexylthiophene) (P3HT, OS2100, Plexcore):phenyl-C_{61}-butyric acid methyl ester (PCBM, 99%, Solenne BV) BHJ spin coated from ortho-dichlorobenzene with 120 °C anneal. We investigated devices with different hole transport layers (HTLs) between the BHJ and the Ag anode (100 nm): 5 nm evaporated MoO_3, 30 nm spin coated poly(3,4-ethylenedioxythiophene):poly(styrenesulfonate) (PEDOT:PSS, Clevios AI4083, Heraeus) with 120 °C anneal, or no HTL. A device with 200 nm P3HT:indene-C_{60} bisadduct (ICBA, 99%, Solenne BV) BHJ and PEDOT:PSS HTL was also fabricated to study the impact of a different donor:acceptor system on SPV. For conventional devices,[24–26] the layer sequence consists of patterned ITO, 30 nm PEDOT:PSS HTL, 200 nm of 1:1 weight ratio P3HT (RMI-001E, Rieke Metals):PCBM BHJ from chlorobenzene, and 100 nm evaporated Al cathode. Three different annealing conditions were chosen: 170 °C for 10 min before Al deposition ("pre-anneal"), 170 °C for 10 min after Al deposition ("post-anneal"), or no anneal. The thermal annealing sequence has been shown to affect V_{oc}.[26] A high V_{oc} conventional device consisting of PEDOT:PSS, 80 nm poly(di(2-ethyl-hexyloxy)benzo[1,2-b:4,5-b′]dithiophene-co-octylthieno[3,4-c] pyrrole-4,6-dione) (PBDTTPD, 1-Material):PCBM BHJ without annealing, 10 nm evaporated Ca, and Al was also studied.[27] V_{oc} values of the devices (0.11 cm^2 area) were determined from current density-voltage (J-V) response measured in N_2 under a class AAA solar simulator (Abet Technologies) with AM1.5G filter at 100 mW cm^{-2} using a low noise source-meter (2635A, Keithley). SPV measurement of the devices was carried out on top of the metal electrode with ITO grounded, using a scanning Kelvin probe (SPS030, KP Technology) with tungsten lamp illumination from the bottom (ITO side) of the sample. All SPV measurements were

[a]Author to whom correspondence should be addressed. Electronic mail: yjalee@utdallas.edu

done in air. Intensities up to 80 mW cm^{-2} were verified using a NREL-calibrated Si photodiode. The large illumination spot size (10 mm) compared to probe size (2 mm) ensured that SPV measurement was conducted under uniform illumination. Surface photovoltage spectroscopy (SPS) was performed by passing the white light through a monochromator to select the illumination wavelength, and measuring the SPV response from 330 nm to 730 nm.

The measurement of contact potential difference (CPD) and SPV is illustrated schematically in Fig. 1, using an inverted P3HT:PCBM BHJ device with ZnO-modified ITO cathode ($\Phi = 4.4$ eV) on bottom and Ag anode ($\Phi = 4.8$ eV after air exposure) on top as an example. When sample and probe are placed in electrical contact, current flows until the Fermi level E_F aligns at equilibrium. This creates an offset in the local vacuum level E_{vac} between Ag top electrode and probe (Fig. 1(a)) with a value equal to eCPD, where e is the elementary charge. In other words, a non-zero electric field exists in the gap between the anode and the probe. Since the stainless steel probe has Φ_{probe} (4.3 eV) $< \Phi_{Ag}$, E_{vac} of Ag is shifted upward relative to E_{vac} of the probe, and we define this CPD to be positive. A dc electrical bias is then applied on the oscillating probe until zero ac current is detected.[14] At this point (Fig. 1(b)), E_{vac} of Ag and the probe aligns, there is zero electric field between the two, and the applied bias equals −CPD. It should be noted that due to the BHJ morphology, the built-in field across the active layer is generated by the E_{vac} offset between the contacts (Fig. 1(a)), which can

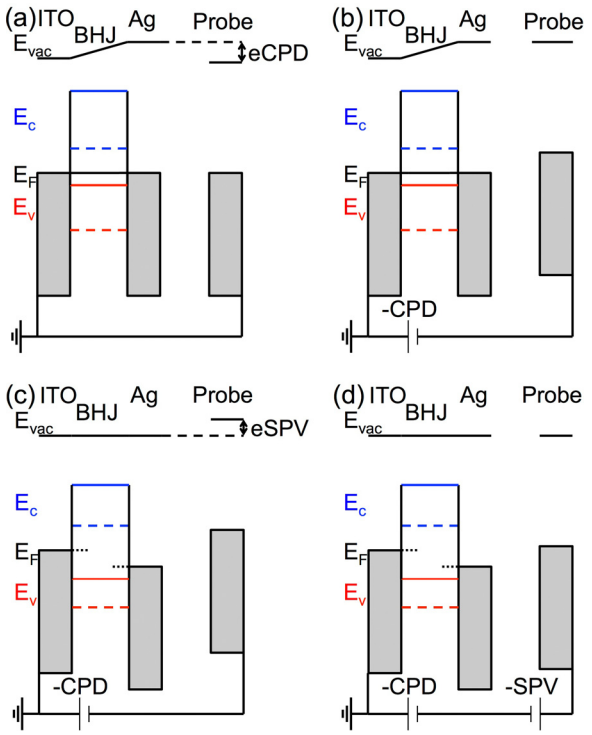

FIG. 1. Schematic of SPV measurement of an inverted P3HT:PCBM BHJ OSC using a Kelvin probe. (a) In darkness at short circuit. (b) In darkness after application of −CPD bias. (c) Under illumination. (d) Under illumination after application of −SPV bias. Valence (E_v, red) and conduction (E_c, blue) band levels are represented for P3HT (solid) and PCBM (dash) in BHJ. Fermi level in equilibrium (E_F, black solid) in equilibrium and quasi-Fermi level under illumination (black dot) are also marked. Grey rectangles represent metals.

be varied with carrier transport layers of different Φ values. Furthermore, CPD between Ag and probe is strongly influenced by charge transfer, band bending, and interfacial dipoles that might exist in the underlying layers.[14] For example, when the BHJ is illuminated, the photogenerated carriers split the quasi-Fermi levels and decrease the magnitude of the built-in field; in Fig. 1(c), the extreme case of flat band condition is shown. The accumulation of holes at the Ag top electrode shifts E_{vac} of Ag downward compared to the case in Fig. 1(b), and a non-zero field in the opposite direction from the field generated by CPD in darkness is found between Ag and the probe. To zero out this field, a bias is then applied to the probe to bring E_{vac} back to alignment (Fig. 1(d)), and CPD under illumination is recorded. SPV is CPD under illumination minus CPD in darkness. Since light illumination reduces the built in field and the CPD, the former is smaller than the latter and SPV is negative. In a conventional device with a low Φ top cathode, the CPD is negative and the accumulation of electrons at the cathode under illumination means that SPV is positive. We note that while Figure 1 illustrates the null signal output condition to simplify the explanation for CPD and SPV, the test instrument (SPS030, KP Technology) utilizes an off-null technique to improve the signal to noise ratio, as detailed in Baikie *et al.*[28] Finally, since the concentration of photogenerated carriers depends on illumination intensity, the magnitude of SPV should increase with illumination intensity until it saturates at maximum quasi-Fermi level splitting, i.e., at flat band condition.

The effect of HTL on the SPV response of inverted OSCs is shown in Fig. 2(a). Below a threshold intensity of ∼0.1 mW cm^{-2}, CPD of all devices remain unchanged from the dark value because the low concentration of photogenerated carriers cannot alter the band bending at the device surface and interfaces, possibly due to incomplete filling of the trap states. The CPD values in the dark for devices without HTL (Fig. 2(a), black) and those with HTL (Fig. 2(a), all others) are 150 mV and 400 mV, respectively. The 250 mV increase in CPD with the insertion of a HTL indicates that E_{vac} of Ag shifts upward when not in direct contact with the BHJ. The resulting increase in the built-in field across the active layer should increase the efficiency of carrier separation, in agreement with HTL improving device performance.[7,10,12] Above the threshold intensity, CPD for the P3HT:PCBM device without HTL (Fig. 2(a), black) decreases linearly with log(intensity), with a slope of −140 mV/decade, and becomes saturated above 0.3 mW cm^{-2}. In comparison, CPD of P3HT:PCBM device with PEDOT:PSS (Fig. 2(a), green) and MoO_3 (Fig. 2(a), green) decreases rapidly as intensity increases to 3 mW cm^{-2}. Above this intensity, CPD decreases linearly with log(intensity), with a slope of −100 mV/decade. Such two-stage response of CPD with intensity was observed previously in crystalline Si solar cells.[15] Since defect energy levels and densities vary from sample to sample, the transition intensity from pinning to non-pinning cannot be calculated or predicted universally. Finally, CPD of P3HT:ICBA device with PEDOT:PSS (Fig. 2(c), blue) shows a qualitatively similar linear dependence with log(intensity), at a slope of −190 mV/decade. The

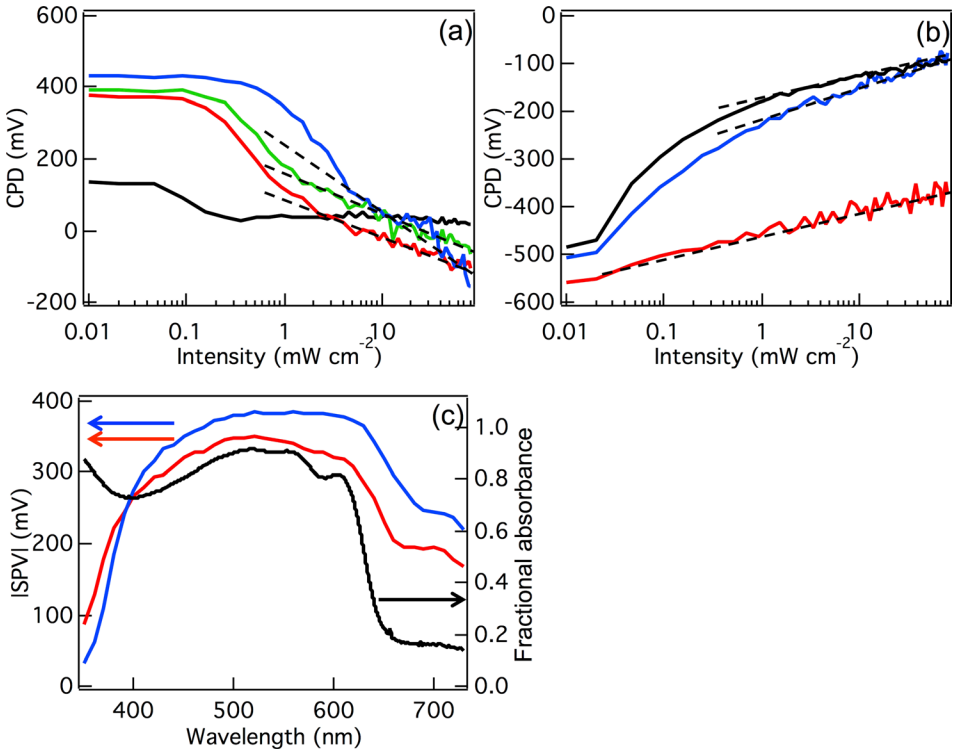

FIG. 2. SPV measurement of OSCs with different interfacial layers and annealing. (a) SPV of inverted P3HT:PCBM without HTL (black), with PEDOT:PSS (red), with MoO_3 (green), and P3HT:ICBA with PEDOT:PSS (blue). (b) SPV of conventional P3HT:PCBM with no anneal (black), pre-anneal (red), and post-anneal (blue). (c) SPS of inverted P3HT:PCBM with PEDOT:PSS (red) and conventional P3HT:PCBM with post-anneal (blue), compared to the fractional absorption spectra (black). The SPV measurement error is ±20 mV.

magnitude of the SPV response has been found empirically to depend on the intensity I via the following equation:

$$|SPV| \cong \frac{\eta kT}{e} \ln(BI), \tag{1}$$

where η and B are proportionality factors.[14] Fitting SPV magnitude of the inverted OSCs to Eq. (1) gives η ranging from 1.5 to 3.2. Such high values are consistent with significant trapping within the bulk of the device.[14] SPV of inverted P3HT:PCBM devices with HTL does not saturate at the maximum illumination intensity of 80 mW cm^{-2}, and at −470 mV to −480 mV is significantly higher in magnitude than the device without HTL (−110 mV), showing that the insertion of HTL enhances accumulation of holes at the anode. Finally, SPV at 80 mW cm^{-2} for the P3HT:ICBA device with PEDOT:PSS (−640 mV) is higher in magnitude by 160 mV compared to the P3HT:PCBM device. This increase agrees well with a 220 meV decrease in the electron affinity of ICBA[29] compared to PCBM,[30] indicating that an increased offset between donor ionization potential and acceptor electron affinity can be detected by SPV measurement.

Next, we examined the effect of thermal annealing on the SPV response of conventional P3HT:PCBM OSCs and found that the order of annealing versus cathode deposition significantly affected photogenerated carrier separation (Fig. 2(b)). At light intensity below 0.01 mW cm^{-2}, CPD of the device annealed before Al electrode deposition ("pre-annealed") is −550 mV, slightly lower than the CPD of the unannealed device and device annealed after Al electrode deposition ("post-annealed") at −500 mV. Typical error in the CPD measurements using the SPS030 system is ±3 mV, and thus the 50 mV difference is outside of experimental error and can be attributed to processing effect. In other words, E_{vac} of the Al cathode on the pre-annealed device exhibits a larger downward shift compared to the other devices, which is expected to improve charge separation by increasing the magnitude of the built-in field across the active layer. With illumination, the SPV response of these conventional OSCs is positive (less negative CPD values), opposite of the inverted devices shown in Fig. 2(a) and consistent with accumulation of photogenerated electrons at the top Al cathode. CPD of the unannealed device (Fig. 2(b), black) increased rapidly between 0.01 and 1 mW cm^{-2}, followed by a linear increase versus log(intensity) with a slope of 40 mV/decade. The post-annealed device (Fig. 2(b), blue) also shows an initial rapid increase and a subsequent linear increase with log(intensity), with a slope of 70 mV/decade. In contrast, CPD of pre-annealed device (Fig. 2(b), red) does not show a clear transition as a function of intensity, and the slope is low at 40 mV/decade, showing that the larger built-in field in the dark does not assist in separating photogenerated carriers. Fit of the SPV response to Eq. (1) gives η ranging from 0.7 to 1.2, suggesting that the conventional devices are limited by surface recombination.[14] It should be noted that the SPV response of the unannealed and post-annealed devices show the characteristic rapid increase at low intensities, followed by a increase that is linear with respect to log(intensity), similar to inverted devices containing HTLs. In contrast, SPV response for the pre-annealed device does not show a clear distinction between the two stages. SPV at 80 mW cm^{-2} gives values of 350 mV, 190 mV, and 430 mV for the unannealed, pre-annealed, and post-annealed devices. These results are consistent with a previous report from Chen *et al.*, who found that the an unannealed P3HT:PCBM BHJ device contained both P3HT and PCBM at the BHJ/Al interface, while pre-annealed device showed enrichment of P3HT and the post-annealed device showed enrichment of PCBM at the same interface.[26] Thus, a PCBM-rich interfacial region between BHJ and Al, which

is present in the unannealed device and enhanced in the post-annealed device, acts as an effective ETL that increases separation of photogenerated carriers and thus SPV.

SPS is performed by measuring the SPV response as a function of illumination wavelength.[14,31] SPS of an inverted P3HT:PCBM device with PEDOT:PSS (Fig. 2(c), red) and a conventional post-annealed P3HT:PCBM device (Fig. 2(c), blue) yields spectra with similar shape that also matches the fractional absorbance spectra (fraction of light absorbed, Fig. 2(c), black). This indicates that absorption of photons by the BHJ and subsequent separation of photogenerated carriers are the main source of the SPV response observed in these devices. The nonzero SPV response at wavelengths greater than the absorption onset (650 nm) may be due to carrier excitation from sub-bandgap trap states and is the subject of future investigation.

We have shown thus far that SPV response of OSCs can be varied from −640 mV to 430 mV for different carrier transport layers, thermal processing, donor:acceptor blends, and device architecture. SPV of inorganic solar cells has been shown to strongly correlate to V_{oc} in two ways. First, by solving the ideal diode equation and assuming that short circuit current density $J_{sc} = b\,I$, where b is a proportionality factor, V_{oc} can be shown to depend on intensity I via[15]

$$V_{oc} \cong \frac{nkT}{e}\ln\left(\frac{J_{sc}}{J_0}\right) = \frac{nkT}{e}\ln I + \frac{nkT}{e}\ln\left(\frac{b}{J_0}\right), \qquad (2)$$

where J_0 is the reverse bias saturation current density. From Eqs. (1) and (2), it can be seen that both SPV and V_{oc} depend linearly on the natural log of illumination intensity. Second, when SPV and V_{oc} of inorganic solar cells were measured at the same intensity, they matched quantitatively.[15,16] In addition to finding a linear dependence between SPV and log(intensity) in a variety of OSCs, a comparison of J-V curves (supplemental material, Figure S1),[32] and Figs. 2(a) and 2(b) show a general correspondence between V_{oc} and SPV. Indeed, when we plot the SPV magnitude measured at 80 mW cm^{-2} versus V_{oc} determined from J-V curves taken at 100 mW cm^{-2} for inverted (Fig. 3, red squares) and conventional (Fig. 3, blue squares) devices, we find a linear correlation between the two values. This provides strong experimental evidence that SPV measures V_{oc} of OSCs.

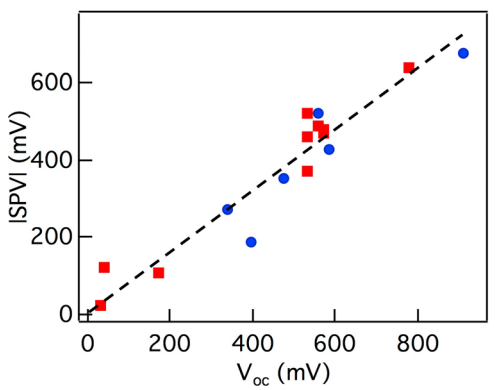

FIG. 3. Plot of SPV magnitude of inverted (red) and conventional (blue) OSCs measured on top of metal electrodes at 80 mW cm^{-2} vs. V_{oc} obtained from J-V curves at 100 mW cm^{-2}, showing strong linear relationship.

In conclusion, Kelvin probe combined with white light and monochromatic illumination were used to examine surface photovoltage of OSCs. Devices with both hole and electron transport layers exhibited a two-stage SPV response versus intensity, with a linear dependence on log(intensity) above a threshold intensity value. Surface photovoltage spectra of inverted and conventional OSCs exhibit similar shape and match well with the absorption spectra, indicating that the surface photovoltage response results from absorption of light by the active layer. Finally, the linear dependence between SPV response and log(intensity) and the agreement between SPV magnitude and V_{oc} for a variety of OSCs indicate that SPV measurement can predict OSC V_{oc} without deposition of top metal contacts, making it an attractive method to perform real-time quality control of OSCs during fabrication, as demonstrated for Si solar cells deposited on flexible steel foil via roll-to-roll processing.[33]

This project was financially supported by the University of Texas at Dallas. The authors thank Professor Iain Baikie and Professor Leeor Kronik for fruitful discussions on the theory of surface photovoltage measurement. J.W.P.H. acknowledges the Texas Instruments Distinguished Chair in Nanoelectronics.

[1]S. Shaheen, D. Ginley, and G. Jabbour, MRS Bull. **30**, 10 (2005).
[2]G. Dennler, M. C. Scharber, and C. J. Brabec, Adv. Mater. **21**, 1323 (2009).
[3]M. Scharber, D. Wuhlbacher, M. Koppe, P. Denk, C. Waldauf, A. J. Heeger, and C. J. Brabec, Adv. Mater. **18**, 789 (2006).
[4]B. P. Rand, D. P. Burk, and S. R. Forrest, Phys. Rev. B **75**, 115327 (2007).
[5]D. Veldman, S. C. J. Meskers, and R. A. J. Janssen, Adv. Funct. Mater. **19**, 1939 (2009).
[6]V. Mihailetchi, P. W. M. Blom, J. Hummelen, and M. Rispens, J. Appl. Phys. **94**, 6849 (2003).
[7]V. Shrotriya, G. Li, Y. Yao, C. Chu, and Y. Yang, Appl. Phys. Lett. **88**, 073508 (2006).
[8]C. Waldauf, M. Morana, P. Denk, and P. Schilinsky, Appl. Phys. Lett. **89**, 233517 (2006).
[9]M. S. White, D. C. Olson, S. E. Shaheen, N. Kopidakis, and D. S. Ginley, Appl. Phys. Lett. **89**, 143517 (2006).
[10]M. D. Irwin, B. Buchholz, A. W. Hains, R. P. H. Chang, and T. J. Marks, Proc. Natl. Acad. Sci. U.S.A. **105**, 2783 (2008).
[11]S. K. Hau, H.-L. Yip, N. S. Baek, J. Zou, K. O'Malley, and A. K. Y. Jen, Appl. Phys. Lett. **92**, 253301 (2008).
[12]Y.-J. Lee, J. Yi, G. F. Gao, H. Koerner, K. Park, J. Wang, K. Luo, R. A. Vaia, and J. W. P. Hsu, Adv. Energy Mater. **2**, 1193 (2012).
[13]H.-L. Yip and A. K. Y. Jen, Energy Environ. Sci. **5**, 5994 (2012).
[14]L. Kronik and Y. Shapira, Surf. Sci. Rep. **37**, 1 (1999).
[15]B. Goldstein, Appl. Phys. Lett. **39**, 258 (1981).
[16]D. J. Szostak and B. Goldstein, J. Appl. Phys. **56**, 522 (1984).
[17]D. J. Ellison, J. Y. Kim, D. M. Stevens, and C. D. Frisbie, J. Am. Chem. Soc. **133**, 13802 (2011).
[18]J. N. Barisci, R. Stella, G. M. Spinks, and G. G. Wallace, Synth. Met. **124**, 407 (2001).
[19]L. Kronik, B. Mishori, E. Fefer, Y. Shapira, and W. Riedl, Sol. Energy Mater. Sol. Cells **51**, 21 (1998).
[20]M. Chiesa, L. Burgi, J. Kim, R. Shikler, R. Friend, and H. Sirringhaus, Nano Lett. **5**, 559 (2005).
[21]H. Hoppe, T. Glatzel, M. Niggemann, A. Hinsch, M. Lux-Steiner, and N. S. Sariciftci, Nano Lett. **5**, 269 (2005).
[22]Y.-Y. Lin, T.-H. Chu, S.-S. Li, C.-H. Chuang, C.-H. Chang, W.-F. Su, C.-P. Chang, M.-W. Chu, and C.-W. Chen, J. Am. Chem. Soc. **131**, 3644 (2009).
[23]E. J. Spadafora, R. Demadrille, B. Ratier, and B. Grevin, Nano Lett. **10**, 3337 (2010).
[24]S. R. Cowan, J. Wang, J. Yi, Y.-J. Lee, D. C. Olson, and J. W. P. Hsu, J. Appl. Phys. **113**, 154504 (2013).

[25]W. Ma, C. Yang, X. Gong, K. Lee, and A. J. Heeger, Adv. Funct. Mater. **15**, 1617 (2005).
[26]D. Chen, A. Nakahara, D. Wei, D. Nordlund, and T. P. Russell, Nano Lett. **11**, 561 (2011).
[27]E. T. Hoke, K. Vandewal, J. A. Bartelt, W. R. Mateker, J. D. Douglas, R. Noriega, K. R. Graham, J. M. J. Fréchet, A. Salleo, and M. D. McGehee, Adv. Energy Mater. **3**, 220 (2013).
[28]I. D. Baikie, K. O. van der Werf, H. Oerbekke, J. Broeze, and A. van Silfhout, Rev. Sci. Instrum. **60**, 930 (1989).
[29]Z.-L. Guan, J. Bok Kim, Y.-L. Loo, and A. Kahn, J. Appl. Phys. **110**, 043719 (2011).
[30]Z.-L. Guan, J. B. Kim, H. Wang, C. Jaye, D. A. Fischer, Y.-L. Loo, and A. Kahn, Org. Electron. **11**, 1779 (2010).
[31]L. Kronik and Y. Shapira, Surf. Interface Anal. **31**, 954 (2001).
[32]See supplementary material at http://dx.doi.org/10.1063/1.4827104 for J-V curves and performance parameters of inverted and conventional OSCs.
[33]B. B. Van Aken, K. J. Bakker, M. C. R. Heijna, D. Reid, I. Baikie, and W. J. Soppe, Phys. Status Solidi A **207**, 682 (2010).